On the design of an ORC axial turbine based expander working as a mechanical driver in gas compressor stations

ON THE DESIGN OF AN ORC AXIAL TURBINE BASED EXPANDER WORKING AS A MECHANICAL DRIVER IN GAS COMPRESSOR STATIONS

Lisa Branchini[1], Cesar Celis[2], Sebastian Ruiz[2], Rene Aguilar[2], Andrea De Pascale[1], Francesco Melino[1]

[1]University of Bologna, Bologna, ITALY
[2]Pontificia Universidad Católica del Perú, Lima, PERU

ABSTRACT

In this work, the feasibility of increasing the capacity of a natural gas compressor station by means of an Organic Rankine Cycle (ORC) is studied. In the proposed configuration, the ORC recovers natural gas compressor drivers' wasted heat and converts it into mechanical energy. Thus, as innovative approach, the ORC generated mechanical power will be used to drag an additional gas compressor. A case study representative of a medium-size on-shore facility is taken as reference. The mechanical drivers' arrangement is composed of four recuperated GTs of PGT5 R type (three units continuously operating and one used as back-up) and two smaller engines of Solar Saturn 20 type. Assuming the actual operation of the station, the addition of an ORC, as bottomer cycle, is designed to recover the exhaust heat from the three PGT5 R running units. According to the Authors' preliminary investigations and state of the art MW-size parameters, a regenerative sub-critical ORC cycle is selected. Therminol 66 and Hexamethyldisiloxane (MM) are chosen as intermediate and working fluids, respectively. The design ORC key cycle parameters are identified: about 2700 hp (2 MW) of capacity could be added to drive a compressor. For a comprehensive investigation, ORC off-design operating range is explored too assuming one out of three topper cycle units out of service. Since a direct coupling of the ORC driver and the gas compressor is expected, thus excluding the use of gearboxes to avoid losses, an ORC axial turbine based expander is designed that accommodates variable speed operation. The referred design includes mean-line calculations and three-dimensional computational fluid dynamics (CFD) based numerical simulations at design and off design point conditions.

Keywords: Organic Rankine Cycle, Waste Heat Recovery, Natural gas compressor station, Mechanical driver, Axial turbine, Preliminary design, CFD modelling.

NOMENCLATURE

Abbreviation

bcma	Billion Cubic Meters per Annum
CFD	Computational Fluid Dynamics
DP	Design point
GT	Gas Turbine
HE	Heat Exchanger
IHTF	Intermediate Heat Transfer Fluid
NG	Natural Gas
OD	Off design point
ORC	Organic Rankine Cycle
REG	Regenerative heat exchanger
WHR	Waste Heat Recovery

Symbols

A	flow area
b	axial chord
C	absolute velocity
c	chord length
D	Diameter
H	blade height
h	specific enthalpy
$\dot{m}$	mass flow rate
N	speed
Nb	Blade number
Ns	specific speed
R	reaction number
SP	size parameter
S	blade pitch
U	Mean peripheral speed
Vr	volumetric expansion ratio
Δ	difference
α	absolute flow angle
β	relative flow angle
θ	stagger angle
ρ	density
i	deviation angle
$\emptyset$	flow coefficient
ψ	stage loading coefficient

Subscripts

a	*axial*
in	*inlet*
out	*outlet*
0	*Stagnation*
1	*Nozzle inlet*

2 *Nozzle outlets*

3 *Rotor outlets*

INTRODUCTION

The world is facing a long-term prospect of a rising demand for energy. Growing population in developing countries will require a massive expansion in energy sources. Natural gas (NG) remains one of the most exploited energetic sources for power production, despite of the important development of sustainable energies over the last years. The International Energy Agency's new gas scenario forecasts that, between 2008 and 2035, primary natural gas demand will increase by 60 % globally [1]. Consequently, natural gas transportation lines are continuously expanding to follow the referred demand. For instance, four major pipeline development initiatives have started globally [2, 3]: 120 billion cubic meters per annum (bcma) is the increasing capacity projected in the North America area, 40 bcma is the one expected in Siberia; 30 bcma are expected to be added to link both Turkmenistan to India and Turkey to Europe.

As highlighted in [4], two growing scenarios can occur: (i) one related to the increase of pipelines capacity by adding more power along them, and (ii) the other involving the addition of new pipelines parallel to the existing ones. The former scenario will require increasing compression station pressure ratios that could be obtained by either replacing single-stage compressors with double-stage units or installing compressors in series to meet the higher pressure ratios. The latter scenario, involving an increase in the gas flow passing through the compression stations, will require installing compressors in parallel to the existing ones.

Therefore, it is of major interest to study solutions to increase both capacity and operating efficiency of natural gas compressor stations, whilst containing climate-change gas emissions. The associated gas compression is usually performed by using centrifugal or reciprocating compressors driven by gas turbines (GTs), electric motors or reciprocated engines. The typical installation arrangement consists of multiple driver units with a potential of operating under part-load conditions and redundant installed capacity in order to ensure both the necessary reserve power and the safe operation of the compressors. In the case of GT drivers, a fraction of transported NG is used as a fuel. The cost of the fuel to be supplied to the gas turbines-based drivers is the main operating cost related to a NG transmission line, reaching up to the 50 % of the company total operating budget [5]. Moreover, due to limited efficiency of the simple cycle gas turbine, large quantities of waste heat are generated during normal operation [2, 5-6]. More details on compressor station typical layouts and drivers requirements can be found in [7-10].

Within this context, this study deals with the possibility of increasing the capacity (in terms of gas mass flow rate) of an existing on-shore compressor station located in the northern part of Italy. As innovative aspect, the increase in station capacity will be accomplished by a waste heat recovery (WHR) technology, thus with a zero-emissions prime mover. As a promising way to enhance the process efficiency, the increase in compressor station capacity is carried out by exploiting gas turbines wasted heat and converting it into mechanical energy through an Organic Rankine Cycle (ORC). Indeed, for heat sources in the temperature range of 300-500 °C, ORC technology represents a competitive and feasible solution for WHR applications, as extensively documented in literature [5, 6, 11].

For this particular and innovative application of ORC as mechanical driver, it must be pointed out that the major challenge relates to the relatively high expander rotational speed required, if gearboxes are to be avoided. Indeed, typical operating speeds for centrifugal compressors in gas transmission applications can be up to 20000 rpm depending on the size [12]. Market available ORC products, conceived for power generation, run however in much lower rotational speeds. ORC expanders' nominal operating speeds are indeed equal to 3600 rpm or 3000 rpm, depending on grid frequency.

Accordingly, an ORC fed with gas turbines wasted heat to be used as additional gas compressor driver is designed in this work. In particular, the main key cycle parameters and the organic fluid are selected to maximize the ORC performance. Once defined the thermodynamic boundary conditions (i.e. design and off-design performance) of the WHR technology, a preliminary design of the ORC expander, mechanically coupled to the driven centrifugal compressor, is carried out. The expander geometry is particularly defined such as to accommodate relatively high rotational speeds (10000 rpm). Notice that in power cycles, axial flow turbines are the preferred solutions to convert working fluid energy into mechanical energy. They are also the most preferred turbines choice in ORC applications featuring power outputs higher than 500 kW [13]. In such applications, organic fluids usually enter the expander at moderate temperatures and perform small isentropic enthalpy drops during the expansion, leading to the design of compact turbines with a reduced number of stages and relatively low stage load coefficients. Moreover, organic fluids usually exhibit large stage volume ratios and a low speed of sound. All of the aforementioned aspects make the design of an ORC turbine a quite challenging task. After preliminarily designing the ORC axial turbine based expander, three-dimensional (3D) computational fluid dynamics (CFD) based numerical simulations of the referred expander are performed here. Summarizing, a feasibility assessment of an ORC coupled to a high speed centrifugal compressor is investigated in order to increase the gas flow rate capacity of a compressor station. The novelty of this work relates to the particular application studied here, the working fluid employed, and the relatively high ORC power rates accounted for.

ORC DESIGN

Case Study Description

A case study representative of a medium-size (24000 hp) on-shore natural gas compressor station is taken as reference

here. Figure 1 shows a scheme of the compressor station actual arrangement. The natural gas arriving at the compressor facility comes from two different off-shore drilling platforms. A low pressure gas stream (LP gas in Figure 1) is compressed into a booster train where two Solar GT units of Saturn 20 type are used as drivers. The latter drag two C160 centrifugal compressors used to raise the gas pressure up to a value compatible with the medium pressure stream (MP gas in Figure 1). The middle pressure gas (combining both streams – the one coming out from the booster train and that one coming from the off-shore platform) enters a gas compressor train made up of three BCL series compressors, each of them driven by a recuperated General Electric PGT5 R machine. A back-up gas turbine unit is included to ensure the necessary reserve of power into the station. The high pressure compressed gas is then sent to the main distribution pipeline. Following the described compressor station arrangement, a significant amount of heat is wasted into the ambient through the GT exhaust gases.

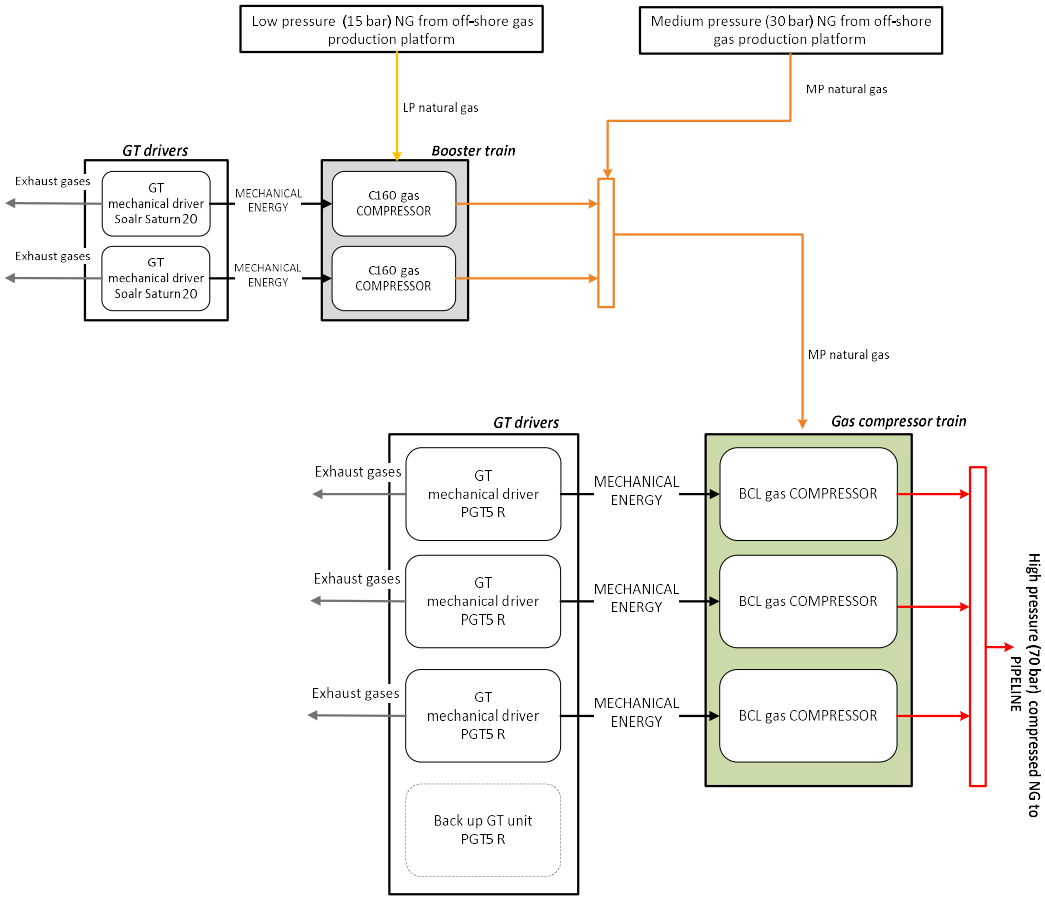

FIGURE 1: NG COMPRESSOR STATION ACTUAL ARRANGEMENT.

ORC Design Assumptions and Results

In order to increase the capacity of the compressor station without adding an additional source of pollutants a WHR technology has been selected. An ORC cycle is thus introduced into the existing compressor station layout, in order to recover the residual heat energy from the three operating PGT5 R units. More specifically, an integrated system is conceived with the GTs train as a topper section and the ORC system as the bottoming cycle, as shown in Figure 2. The regenerative sub-critical bottomer cycle features an intermediate oil circuit separating the GTs exhaust gases and the organic fluid related circuit. A numerical model of the integrated plant – both at design and off-design point conditions – has been developed by means of Thermoflex [14] (more details can be found in [2, 5, 15]). This software, according to a lumped parameters approach, allows for the thermodynamic modelling of power plants, starting from built-in library single components assembly. Properties of intermediate and organic fluids are evaluated according to the Refprop thermodynamic database.

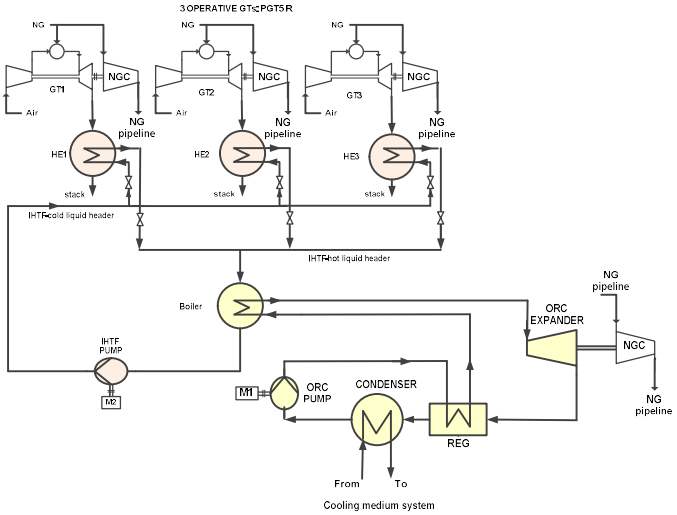

FIGURE 2: GTS-ORC WASTE HEAT RECOVERY LAYOUT.

The performance of the bottomer cycle is determined through three main consecutive steps: i) a thermodynamic design analysis where the cycle layout, boundary conditions and design assumptions are given as inputs, and the software utilized here computes preliminary heat and mass balances; ii) the engineering design phase where component sizes and main geometric details are calculated; and iii) the off-design analysis stage where, being defined the design characteristics and fixed the geometry of the components, depending on selected control logics, it is possible to predict both components and overall system behavior under different operating conditions, thus obtaining off-design performance.

The ORC has been designed such as to maximize the mechanical power output keeping the main key cycle parameters in line with manufacturer's state-of-the art values and Authors' preliminary investigations [5, 15]. Therminol 66 and Hexamethyldisiloxane (MM) have been chosen as intermediate (IHTF) and working fluids, respectively (relevant thermodynamic properties are summarized in Table 1).

For this specific application, the choice of the organic fluid has been also influenced by concerns on the expander design. Indeed, the large molecular mass (162 g/mol) of MM is beneficial for the turbine design since the molecular mass value is inversely proportional to the expander enthalpy drop, meaning that heavy molecules require lower number of stages and/or lower peripheral speeds and mechanical stresses [13].

The main assumptions of the topper-bottomer integrated cycle, input for the thermodynamic design analysis, are summarized in Table 2.

TABLE 1: ORGANIC FLUID AND IHTF MAIN PROPERTIES.

MM (Hexamethyldisiloxane)	
Molar weight [g/mol]	162.38
Critical Pressure [bar]	19.1
Critical Temperature [°C]	245
Density [g/cm^3]	0.764
Thermal stability limit [°C]	290
IHTF (Therminol 66) property	
Molar weight [kg/kmol]	252
Maximum bulk temperature [°C]	345
Maximum film temperature [°C]	375
Normal boiling point [°C]	359
Autoignition temperature [°C]	374
Liquid density at 15°C [kg/m3]	1012

TABLE 2: GTs-ORC DESIGN ASSUMPTIONS.

GTs section	
GT exhaust temperature @ full load [°C]	364
GT exhaust mass flow (single unit) @ full load [kg/s]	25.35
Minimum GT stack temperature [°C]	150
ORC section	
ORC expander isentropic efficiency [%]	80
ORC evaporative pressure-critical pressure ratio [-]	0.76
Organic fluid superheating degree [°C]	15
HE pressure drop IHTF / gas side [bar]	2/0.015
IHTF maximum temperature [°C]	315
Boiler pressure drop IHTF/ organic fluid [bar]	1/1.5
REG effectiveness [%]	80
REG pressure drop ORC liquid/vapor side [bar]	0.2/0.15
Subcooling ORC outlet condenser [°C]	5
Condensation pressure [bar]/ temperature [°C]	1/100
Cooling medium ΔT in condenser [°C]	15
Condenser pressure drop, cooling medium side [bar]	0.2
Miscellaneous	
Heat exchangers thermal loss [%]	1
Pumps mechanical efficiency [%]	80
Minimum pinch point assumed in HEs [°C]	7

For the organic fluid, as evaporative pressure over critical pressure and superheating temperature over critical temperature, values equal to 0.76 and 1.02 have been selected, respectively. The isentropic efficiency of ORC expander has been set equal to 80 %, in line with MW-size ORC commercial units [15]. Similar consideration is for the regenerative heat exchanger effectiveness assumed, equal to 80 %. Pressure drops at intermediate heat exchangers, boiler and condenser are specified according to commercial components data. Finally, GT stack temperature, after the waste heat recovery section, has been limited to 150 °C.

ORC off-design cycle assessments have been carried out assuming sliding pressure regulation for the axial expander, thermal resistance scaling, as the method to reproduce heat exchangers off-design behavior, and flow resistance coefficients, initialized at design-point, to model fluids' pressure drops across components. More details on bottomer cycle off-design modelling can be found in [5].

The most relevant bottomer cycle performance results, both at design and off-design (two out of three GT units working) point conditions are listed in Table 3.

TABLE 3: ORC CYCLE RESULTS.

	DESIGN	***OFF-***

		DESIGN
EXPANDER PARAMETERS		
Expander inlet pressure [bar]	14.00	9.75
Expander inlet pressure (after valve) [bar]	12.6	8.8
Expander inlet temperature [°C]	250	250
Expander inlet flow [kg/s]	47.57	31.19
Expander inlet specific volume [m^3/kg]	0.014	0.023
Expander outlet pressure [bar]	1.15	0.595
Expander outlet temperature [°C]	213	215
Expander outlet specific volume [m^3/kg]	0.211	0.415
Actual pressure ratio (including valve pressure drops) [-]	10.96	14.74
Expander size parameters [m]	1.15	1.26
Expander volume ratio [-]	15.47	18.38
Expansion power [kW]	2099	1621
OVERALL CYCLE PARAMETERS		
Shaft power [kW]	1993	1516
Thermal power input to ORC cycle [kW]	13338	9373
Thermal power rejected in the condenser [kW]	11236	7770
ORC first law efficiency [-]	0.149	0.162

At design point, the ORC is capable of generating about 2700 hp (2 MW) of additional mechanical power output, recovering 13 MW of heat. Bottomer cycle first law efficiency results close to 15 %. As a consequence, comparing the thermal efficiency of the proposed GTs-ORC setup with the existing one (GTs stand-alone) and increase of 2 percentage points is obtained thanks to the addition of the WHR system.

From the environmental point of view, the impact of ORC is relevant also in terms of CO_2 avoided emissions. Indeed, comparing to the use of a 2 MW class gas turbine (with a reference thermal efficiency of 30 %), the implementation of the WHR solution allows for a saving of about 1.3 tons of carbon dioxide per hour of compressor station operation. Please refers to [15] for additional details on CO_2 calculation.

Focusing on ORC expander results, entry conditions in terms of flow inlet pressure (before valve) and temperature are 14 bar and 250 °C, respectively. Expander exit conditions are, in turn, 1.15 bar and 213 °C.

Reducing the amount of available heat to be recovered by the ORC due to the compressor station off-design operation, the power output is reduced in about 20 % when compared to the design value. This is due to the decrease of both the working fluid mass flow rate and the specific work. In contrast, the expander actual pressure ratio is increased from 11 to 15, mainly due to the more significant decrease of the expander inlet pressure.

The results of the thermodynamic analysis carried out (i.e. expander inlet and outlet conditions) provide the design requirements for the axial machine capable of accommodating high speed operation, as detailed in the following paragraphs. Notice that no design related iterative processes including both the ORC cycle and the expander geometry have been carried out here.

ORC EXPANDER PRELIMINARY DESIGN

In this section, an ORC axial turbine based expander accommodating relatively high speed operation is preliminarily designed. The referred ORC expander preliminary design is carried out using a mean-line [16] based approach. This design approach aims to obtain the associated flow velocity triangles and an initial blade geometry. For the design process, the expansion system has been thus simplified to a single dimension by taking as reference an expander mean diameter. The calculation procedure used here is similar to that used in previous works [13, 16-17]. The input parameters accounted for include the flow properties at the expander inlet and outlet, as well as the expander mass flow rate (see Table 3). Other parameters required for the expander preliminary design have been also considered when necessary. These parameters, which are summarized in Table 4, include the expander rotational speed (N), reaction degree (R), flow coefficient (∅), mean diameter (Dmean) and number of stages (Nstages).

TABLE 4: ADDITIONAL PARAMETERS CONSIDERED.

	Symbol	*Value*
Rotational speed [RPM]	N	10000
Reaction degree	R	0.5
Flow coefficient	∅	0.95
Mean diameter [m]	Dmean	0.20
Number of stages	Nstages	2

As part of the expander preliminary design process, in order to approximate the velocity triangle profiles, the dimensionless parameters highlighted in Eqs. (1-3) were initially computed. Charts elaborated by Macchi et. al [13] involving the dimensionless parameters described in Eqs. (4-6) were then used to estimate an initial expander efficiency. Notice that Eqs. (1) to (3) represent, respectively, flow coefficient (∅), stage loading coefficient (ψ) and reaction number (R). Eqs (4) to (6) involve in turn the size parameter (SP), the volumetric expansion ratio (Vr) and the specific speed (Ns).

$$\emptyset = \frac{Ca}{U} \tag{1}$$

$$\psi = \frac{\Delta h_0}{U^2} \tag{2}$$

$$R = \frac{\Delta h_{rotor}}{\Delta h_{stage}} \tag{3}$$

$$SP = \frac{{V_{out}}^{0.5}}{{\Delta h_{stage}}^{0.25}} \quad (4)$$

$$Vr = \frac{V_{out}}{V_{in}} \quad (5)$$

$$Ns = \left[\frac{{V_{out}}^{0.5}}{{\Delta h_{stage}}^{0.75}}\right] \times \left(\frac{N}{60}\right) \quad (6)$$

Following [16], the relations used to construct the velocity diagrams include those determining the inlet and outlet flow angles, Eqs. (7-10),

$$tan\alpha_2 = \frac{\left[\frac{\psi}{2} + (1 - R)\right]}{\emptyset}, \quad (7)$$

$$tan\alpha_3 = \frac{-\left[\frac{\psi}{2} - (1 - R)\right]}{\emptyset}, \quad (8)$$

$$tan\beta_2 = \frac{-\left(\frac{\psi}{2} - R\right)}{\emptyset}, \quad (9)$$

$$tan\beta_3 = \frac{\left(\frac{\psi}{2} + R\right)}{\emptyset}, \quad (10)$$

and the stage velocities, Eqs. (11-14),

$$C2 = U\sqrt{\left[(1 - R) + \frac{\psi}{2}\right]^2 + \emptyset^2}, \quad (11)$$

$$C3 = U\sqrt{\left[(1 - R) - \frac{\psi}{2}\right]^2 + \emptyset^2}, \quad (12)$$

$$W2 = U\sqrt{\left[\frac{\psi}{2} - R\right]^2 + \emptyset^2}, \quad (13)$$

$$W3 = U\sqrt{\left[\frac{\psi}{2} + R\right]^2 + \emptyset^2}. \quad (14)$$

In this work an initial inlet flow angle equal to 0° was accounted for. A scheme of the velocity triangle profiles determined here is shown in Figure 3.

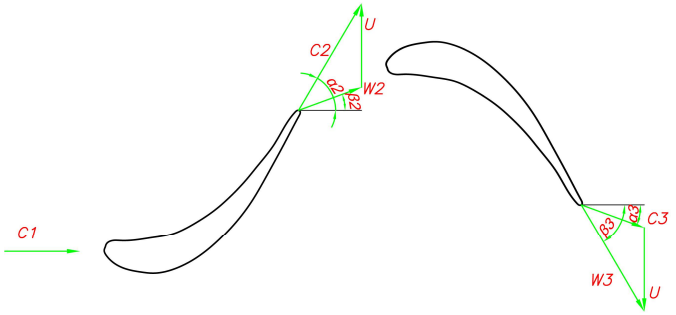

FIGURE 3: VELOCITY TRIANGLES SCHEME.

The next step involved determining an approximated blade geometry. Accordingly, by estimating the blades height, Eq. (15),

$$H = \frac{\dot{m}}{\pi Dmean\rho\emptyset U}, \quad (15)$$

and the blades hub and tip diameters, Eqs. (16-17),

$$Dhub = Dmean - H, \quad (16)$$

$$Dtip = Dmean + H, \quad (17)$$

the expander annular geometry was firstly defined. This was followed by the calculation of the blade axial chord length, Eq (18),

$$b = c \times \cos\theta, \quad (18)$$

and the number of blades, Eq. (19),

$$Nb = \frac{\pi Dmean}{S} \quad (19)$$

Notice that values for the blades pitch to chord ratio and aspect ratio usually suggested in literature were accounted for. Blade chord, pitch, axial chord length, solidity and number of blades were estimated following references [16, 17]. The stagger angle was taken from the diagram provided in [17], although this is a highly iterative parameter. Since flow relative angles are not necessarily equal to blade angles, a deviation angle (i), Eq. (20), had to be calculated. Finally, axial Mach numbers (less than 1.4) and hub to tip ratios (less than 0.9) were verified in order to preliminary design a feasible axial turbine.

$$i = 14° \left(1 - \frac{\alpha_{in}}{70°}\right) + 9° \left(1.8 - \frac{c}{S}\right) \quad (20)$$

The values of main parameters characterizing the ORC axial turbine based expander preliminarily designed here are summarized in Tables 5-7. These parameters include the dimensionless ones accounted for in this work (Table 5), the blade geometry ones (Table 6), and the annulus geometry related parameters (Table 7). As highlighted in the referred tables, the ORC axial turbine features two stages, and the tip diameters along the expander vary from about 21 to 36 cm. The

number of stator/rotor blades in the first and second stages are equal in turn to 30/29 and 18/13, respectively.

TABLE 5: DIMENSIONLESS PARAMETERS

	Symbol	*1st stage*	*2nd stage*
Size Parameter	SP	0.14	0.26
Volume Ratio	VR	3.95	3.39
Specific Speed	Ns	0.16	0.3
Isentropic Efficiency	η	0.80	0.80

TABLE 6: BLADE GEOMETRY PARAMETERS

	Symbol	*Stator 1*	*Rotor 1*	*Stator 2*	*Rotor 2*
Pitch to chord ratio	S/c	0.86	0.8	0.8	0.82
Aspect ratio	h/c	1	1.7	2	2.6
Stagger Angle	-	36	29	30	30
Chord Length [mm]	c	25	28	44	61
Pitch Length [mm]	S	21	22	35	50
Number of Blades	Nb	30	29	18	13
Axial chord [mm]	b	20	24	38	53

TABLE 7: ANNULUS GEOMETRY PARAMETERS

	Stator 1 inlet	*Rotor 1 inlet*	*Stator 2 inlet*	*Rotor 2 inlet*	*Stator 2 outlet*
Tip diameter [mm]	212	225	247	287	360
Hub diameter [mm]	188	175	153	113	40
Blade height [mm]	12	25	47	87	160
Hub to tip ratio	0.89	0.78	0.62	0.39	0.11

ORC EXPANDER 3D CFD SIMULATIONS

In this section, 3D CFD simulations at design and off design point conditions of the ORC axial turbine based expander previously designed are discussed. The particular off design point condition studied here correspond to the case in which only two out of three GT units provide the heat required to operate the ORC based plant (Table 3).

General aspects

The main purpose of the expander CFD numerical simulations carried out is to highlight the qualitative features of the fluid flow passing through the designed axial turbine based expander. Mach number and pressure distributions as well as flow patterns characterizing the axial expander are thus particularly discussed in this section. Accordingly, as part of the pre-processing stage of the CFD analyses performed, the expander (rotor and stator) geometry, preliminarily defined using a mean-line approach, was firstly created using the commercial package Ansys Design Modeler [18]. The resulting expander stator and rotor geometries are shown in Figure 4.

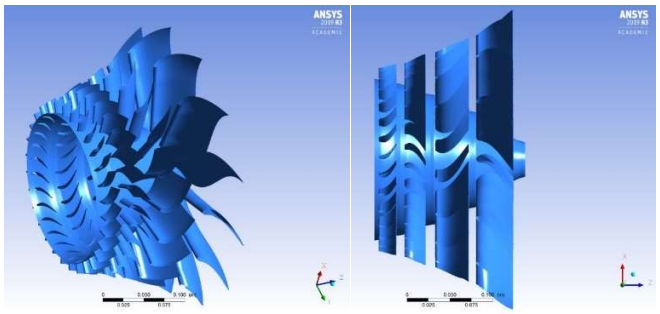

FIGURE 4: EXPANDER STATOR AND ROTOR GEOMETRIES.

The 3D stator and rotor blade geometries initially created were then exported to the mesh generator utilized here. In this work Ansys Turbogrid [19] was used to generate structured H-O meshes for both stators and rotors. In order to determine mesh independent results, three different computational meshes were initially tested. The mesh independence analysis carried out was based on the computing of the total force exerted by the fluid flow on the expander rotor 2 blades. The expander second rotor was accounted for here because of its size and the relatively high Mach numbers characterizing it. As shown in Table 8, the rotor meshes studied here feature numbers of elements ranging from 1.2 to 2.4 million elements. Even though the most refined mesh almost doubles in size to the coarsest one, the relative differences in terms of total force are less than 0.7 % (Table 8). The coarsest rotor mesh (Mesh 1) has been therefore utilized as the basis for generating the expander mesh used in the simulations performed in this work. More specifically, the same parametrization criteria used in the rotor 2 mesh have been applied to generate the meshes for the remaining expander rotor and stators. The so obtained meshes have been further refined in the radial direction to decrease the edge length ratio and to ensure a proper boundary layer description. Details of the computational meshes utilized here are highlighted in Figures 5 and Table 9. As noticed from this last table, the expander mesh utilized here features about 4.64 million elements.

TABLE 8: ORC EXPANDER ROTOR 2 MESH INDEPENDENCE

	No. of mesh elements [Millions]	*Total force [N]*	*Diff. [%]*
Mesh 1	1.21	811.5	0.67
Mesh 2	1.75	809.9	0.47
Mesh 3	2.40	806.1	0.00

TABLE 9: ORC EXPANDER MESH SIZE

	Stator 1	*Rotor 1*	*Stator 2*	*Rotor 2*	*Total*
No. of mesh elements [Millions]	0.98	1.02	1.27	1.37	4.64

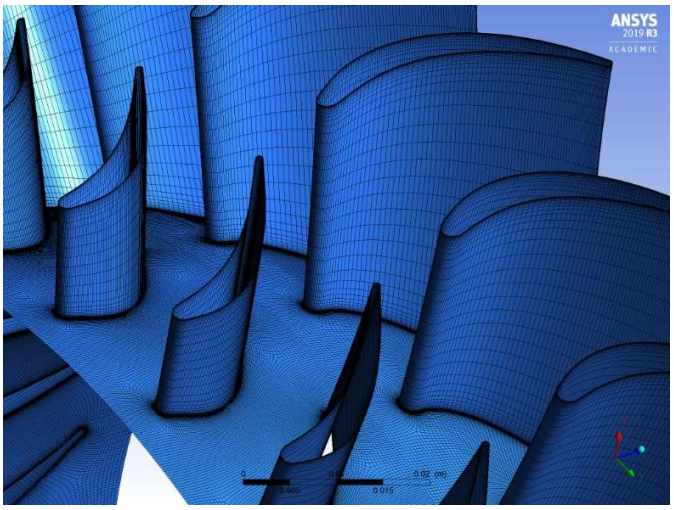

FIGURE 5: EXPANDER COMPUTATIONAL MESH.

The steady state numerical simulations performed in this work involved the use of the Ansys Fluent solver [20]. This solver has been chosen here due to its proved performance to simulate organic fluids, through the coupling of the NIST REFPROP library [21], which is required to properly represent organic fluid real gas properties. All numerical simulations carried out involved a pressure-based scheme along with a $k-\omega$ SST [22] turbulence model. A mixing planes based approach was used to account for rotor-stator interactions. This method has a demonstrated capability to represent turbomachinery rotor-stator coupling effects [23].

ORC cycle parameter values (Table 3) were used as boundary conditions to the expander computational domain simulated here. In addition, at design point, an expander rotational speed equal to 10000 RPM was accounted for. For the off design point condition numerically simulated here in turn, the rotational speed was reduced to 90 % of the nominal one (design point). Due to the several convergence issues observed during the numerical simulations carried out, progressively increasing expander pressure drops were utilized. Furthermore, the expander rotational speed was also progressively increased to avoid pressure and temperature fluctuations leading to divergence related problems. The main results obtained at design and off design point conditions are highlighted below.

Design point (DP) results

Contours of Mach number, static pressure and total temperature characterizing the ORC axial turbine based expander designed here at design point conditions are shown in Fig. 6, Fig. 7 and Fig. 8, respectively. In particular, from Fig. 6 it is seen that, as expected, the flow accelerates as it passes through the stator vanes. A similar situation occurs in the rotor blades although this is not so evident from the referred figure.

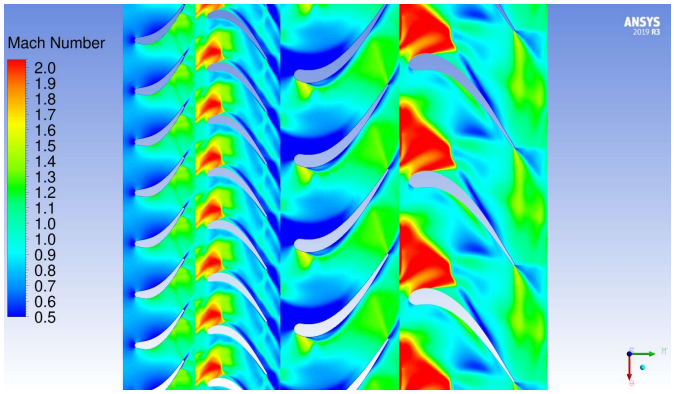

FIGURE 6: EXPANDER MACH NUMBER DISTRIBUTION – DESIGN POINT.

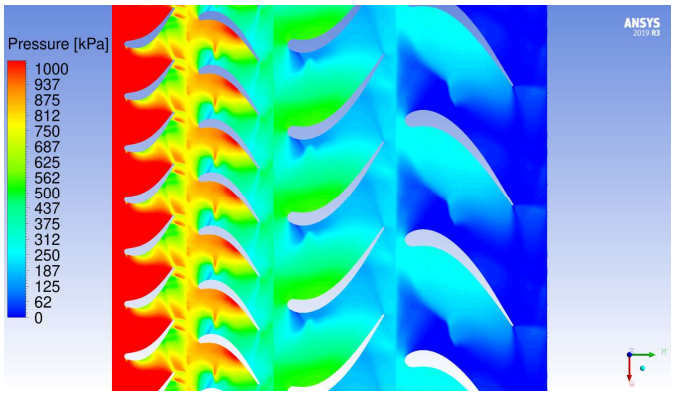

FIGURE 7: EXPANDER STATIC PRESSURE DISTRIBUTION – DESIGN POINT.

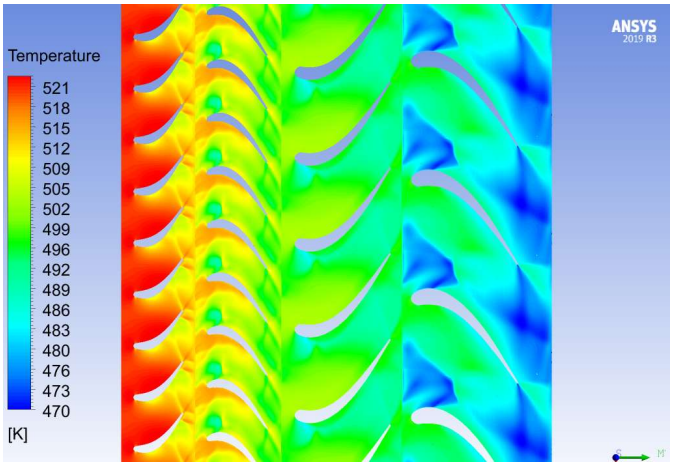

FIGURE 8: EXPANDER TOTAL TEMPERATURE DISTRIBUTION – DESIGN POINT.

In terms of pressure, Fig. 7 shows that the flow regions presenting the highest pressure values are those located on the pressure side of both stator vanes and rotor blades. These flow regions correspond of course to the locations where the lowest flow velocities (Fig. 6) are found. It is also possible to see from Fig. 7 that pressure decreases along the expander axial direction. This aspect is further emphasized by the results included in Fig. 9, which shows the variation of the static pressure along the mid plane of the ORC expander designed here. The expander total temperature (Fig. 8) also decreases as the flow expands through the turbine stages accounted for.

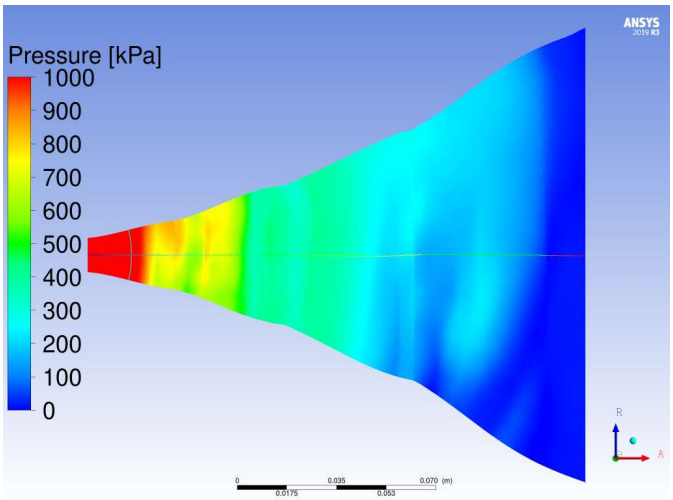

FIGURE 9: VARIATION OF STATIC PRESSURE ALONG THE EXPANDER AXIAL DIRECTION – DESIGN POINT.

Finally, Fig. 10 and Fig. 11 show the pressure distribution (blade loading) on the 1st and 2nd stage rotors at 50 % span. From these figures, it can be seen that at design point conditions relatively smooth pressure distributions characterize the pressure surfaces of both rotors. Something similar occurs on the suction surface of the first rotor. The suction side of the second rotor presents however some pressure fluctuations. Refinements in the ORC expander geometry will be carried out in future in order to improve these pressure distributions along both pressure and suction surfaces.

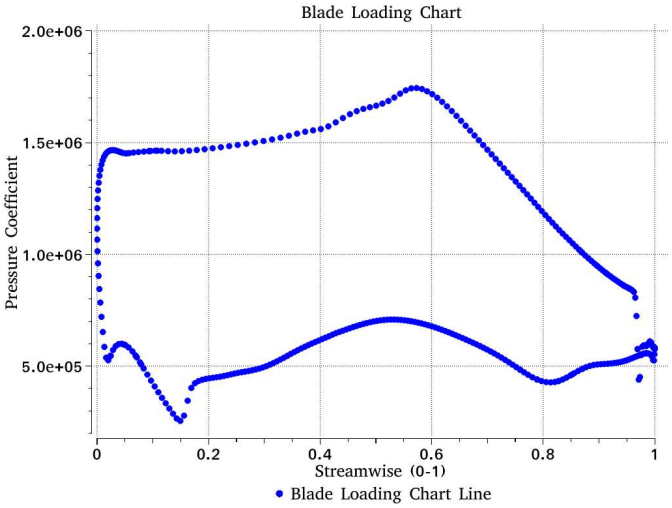

FIGURE 10: BLADE LOADING FOR 1ST STAGE ROTOR – DESIGN POINT.

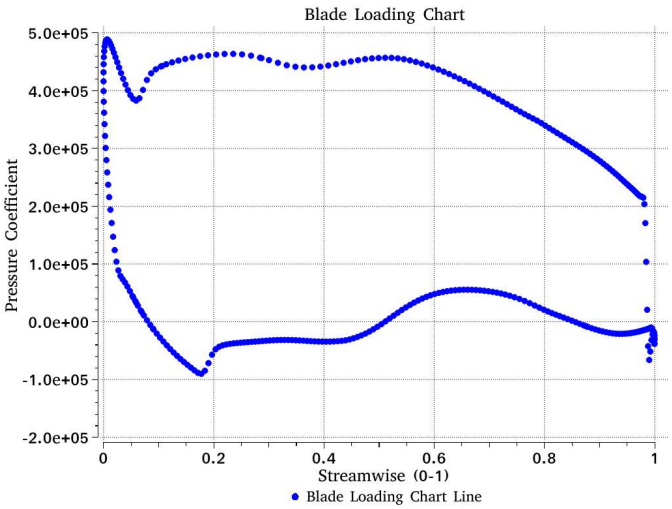

FIGURE 11: BLADE LOADING FOR 2ST STAGE ROTOR – DESIGN POINT.

Off design point (OD) results

The results at off design point conditions, in terms of Mach number and static pressure, are shown in Fig. 12 and Fig. 13, respectively. As observed from these figures, the illustrated contours are similar to the corresponding ones shown in Fig. 6 and Fig. 7 above. Notice however that overall both the Mach numbers and the pressure levels at design point are higher than at off design. This Mach number behavior can be particularly observed from the associated contours characterizing the fluid flow as it passes through the ORC expander rotors.

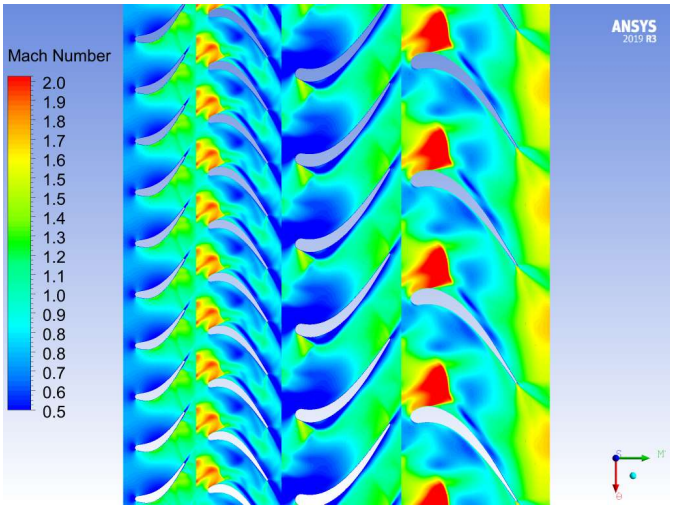

FIGURE 12: EXPANDER MACH NUMBER DISTRIBUTION – OFF DESIGN.

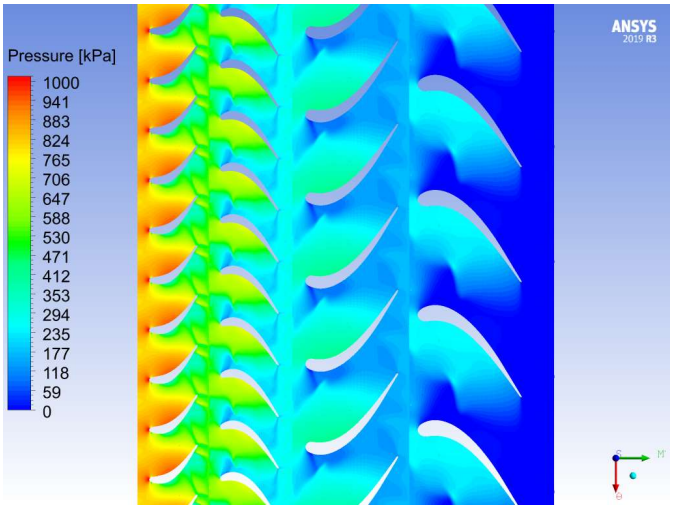

FIGURE 13: EXPANDER STATIC PRESSURE DISTRIBUTION – OFF DESIGN.

Similarly to what is illustrated in Fig. 10 and Fig. 11, Fig. 14 and Fig. 15 show respectively, at off design conditions, the pressure distribution (blade loading) on the 1st and 2nd stage rotors at 50 % span. It is firstly noticed from Fig. 14 that at off design the blade loading on the first rotor pressure surface largely decreases. This reduction in pressure coefficient is expected to lead to ORC expander power output decreases. In addition, Fig. 15 shows that at off design some pressure fluctuations remain on the second rotor suction side. Interestingly, as noticed from Fig. 14 and Fig. 15, the pressure surfaces of both rotors keep free from pressure fluctuations at the particular off design point condition analyzed here.

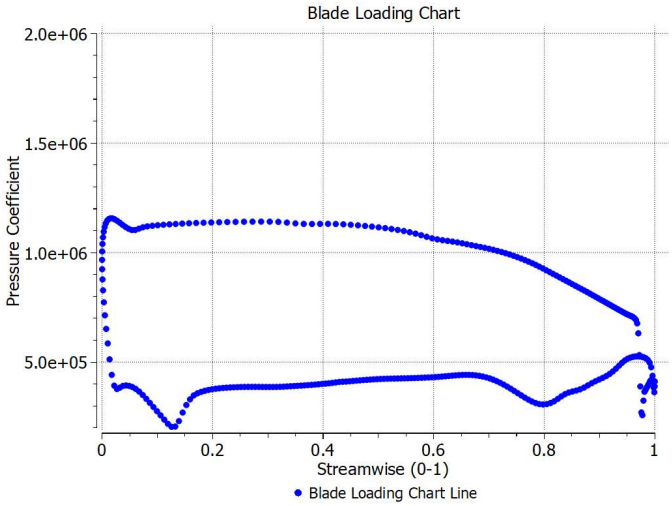

FIGURE 14: BLADE LOADING FOR 1ST STAGE ROTOR – OFF DESIGN.

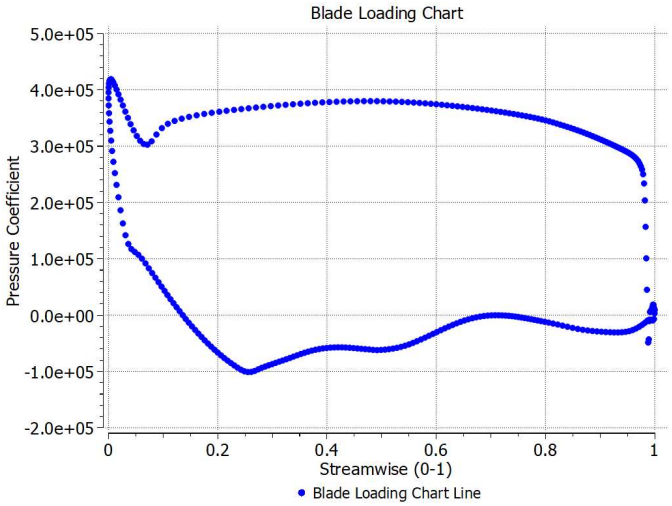

FIGURE 15: BLADE LOADING FOR 2ST STAGE ROTOR – OFF DESIGN.

The CFD based overall parameters characterizing the designed expander are summarized in Table 10. For comparison purposes, this table also includes those parameters coming from the cycle analyses initially carried out (Table 3). As noticed from this table, the ORC axial turbine based expander designed in this work is capable of producing a thermodynamic power output of about 1.88 MW. Compared to the ORC cycle results and accounting for design and off design point conditions, the CFD results present average discrepancies ranging from 5 to 14 %, approximately. Considering that cycles analyses and mean line based design approaches provide only preliminary results, the discrepancies shown in this table seems to be reasonable. Indeed, carrying out design optimization processes, involving for instance iterative processes between the expander preliminary design and the corresponding CFD assessments, these discrepancies can be eventually reduced.

TABLE 10: QUANTITATIVE CFD RELATED RESULTS

	Cycle		*CFD*		*Average discrepancy [%]*
	Design	***Off design***	***Design***	***Off design***	
Mass flow rate [kg/s]	47.57	31.19	43.20	31.00	4.9
Pressure Ratio [-]	10.96	14.74	11.36	12.53	9.3
Expansion Power Output [MW]	2.10	1.62	1.88	1.33	14.1
Isentropic Efficiency	0.80	0.80	0.824	0.820	2.8

CONCLUSIONS

This paper investigates the feasibility of an innovative application of an organic Rankine cycle as mechanical driver of a centrifugal compressor. For the purpose of the study, a case study representative of a medium-size (24000 hp) on-shore natural gas compressor station is taken as reference. The proposed ORC bottomer cycle is designed to maximize its mechanical power output recovering the exhausted heat from three *PGT5 R* type running units. A regenerative sub-critical and superheated cycle is defined. Therminol 66 and Hexamethyldisiloxane are chosen as intermediate and working fluids, respectively. A numerical model of the integrated plant – both at design and off-design point conditions – has been developed. The thermodynamic analysis results of show that the ORC is capable of generating about 2700 hp (2 MW) of additional mechanical power, recovering 13 MW of heat. Bottomer cycle first law efficiency results close to 15 %. ORC expander entry conditions in terms of flow inlet pressure and temperature are 14 bar and 250 °C, respectively. Expander exit conditions are, in turn, 1.15 bar and 213 °C.

Design expander inlet and outlet conditions have been used, as boundary conditions, for defining the axial expander geometry by means of mean-line calculations and three-dimensional computational fluid dynamics based numerical simulations. Indeed, since a direct coupling of the ORC driver and the gas compressor is expected the axial machine is designed, for this specific application, to accommodate high speed (10000 rpm) operation. A two stage axial expander is identified. The tip diameters along the expander vary from about 21 to 36 cm. The number of stator/rotor blades in the first and second stages are equal to 30/29 and 18/13, respectively. Results of the CFD modelling at design and off design point conditions, according to Mach number distribution, confirm that the flow accelerates as it passes through the stator vanes. Pressure distribution results show that the flow regions presenting the highest pressure values are those located on the pressure side of both stator vanes and rotor blades. These regions correspond of course to the locations where the lowest flow velocities are found. Temperature and pressure distributions show decreasing values along the expander axial direction, as expected.

The calculated enthalpy variation across the first and second stages of the designed axial expander confirms the possibility to generate about 2 MW of additional power.

REFERENCES

[1] International Energy Agency (IEA) new gas scenario https://www.iea.org/weo2018/scenarios/ (Accessed in November 2019)

[2] L. Branchini, M. A. Ancona, M. Bianchi, A. De Pascale, F. Melino, A. Peretto, S. Ottaviano, N. Torricelli, D. Archetti, N. Rossetti, T. Ferrari. Optimum Size of ORC Cycles for Waste Heat Recovery in Natural Gas Compressor Stations. Proceedings of ASME Turbo Expo 2019: June 17-21, 2019, Phoenix, Arizona, USA. GT2019-90009

[3] Global gas report 2018, World Gas Conference 2018, http://www.snam.it/it/gas-naturale/global-gas-report/

[4] R. Kurz. On compressor station layout. Proceedings of ASME Turbo Expo 2003: Turbomachinery Technical Conference and Exposition, Paper No. GT2003-38019.

[5] M. Bianchi, L. Branchini, A. De Pascale, F. Melino, A. Peretto, D. Archetti, F. Campana, T. Ferrari, N. Rossetti. Feasibility of ORC application in natural gas compressor stations. Energy, 2019, Vol. 173, pp: 1-15, doi:10.1016/j.energy.2019.01.127.

[6] F. Campana, M. Bianchi, L. Branchini, A. De Pascale, A. Peretto, M. Baresi, A. Fermi, N. Rossetti, R. Vescovo. ORC Waste Heat Recovery in European Energy Intensive Industries: Energy and GHG Savings. Energy Conversion and Management, 2013, Vol. 76, pp. 244–252. doi: 10.1016/j.enconman.2013.07.041.

[7] R. Kurz, S. Ohanian, M. Lubomirsky, On compressor station layout. (2003) American Society of Mechanical Engineers, International Gas Turbine Institute, Turbo Expo IGTI, 4, pp. 1-10. DOI: 10.1115/GT2003-38019

[8] R. Zamotorin, R. Kurz, D. Zhang, M. Lubomirsky, K. Brun, Control optimization for multiple gas turbine driven compressors, (2018) Proceedings of the ASME Turbo Expo, 9, DOI: 10.1115/GT2018-75002

[9] R. Kurz, K. Brun, Process control for compression systems (2017) Proceedings of the ASME Turbo Expo, GT2017-63005, DOI: 10.1115/GT2017-63005.

[10] R. Kurz, M. Lubomirsky, Concepts in gas compressor station configuration, (2012) Society of Petroleum Engineers - International Petroleum Technology Conference 2012, IPTC 2012, 1, pp. 733-742.

[11] Gómez-Aláez, S. L., Brizzi, V., Alfani, D., Silva, P., Giostri, A., Astolfi, M. Off-design study of a waste heat recovery ORC module in gas pipelines recompression station, Energy Procedia, Vol. 129, (2017), pp:567-574, doi: 10.1016/j.egypro.2017.09.205.

[12] M. Stewart, Pump and Compressor Systems: Mechanical Design and Specification, Surface Production Operations, Volume IV - 2019, pp: 457-525, DOI: 10.1016/C2009-0-20243-1, ISBN:978-0-12-809895-0.

[13] E. Macchi, M. Astolfi. Organic Rankine Cycle (ORC) Power Systems- technologies and applications, Woodhead

Publishing series in energy, 107, Elsevier, 2017, ISBN: 978-0-08-100510-1.
[14] Thermoflex 27.0, 2019, Thermoflow Inc., Sudbury, MA, USA.
[15] Bianchi, M., Branchini, L., De Pascale, A., Melino, F., Orlandini, V., Peretto, A., Archetti, D., Campana, F., Ferrari, T., Rossetti, N. Energy Recovery In Natural Gas Compressor Stations Taking Advantage Of Organic Rankine Cycle: Design Analysis, Proceedings of ASME Turbo Expo 2017: Turbomachinery Technical Conference and Exposition, Paper No. GT2017-64245, pp. V009T27A016; 14 pages, doi:10.1115/GT2017-64245
[16] Dixon , SL, Hall, C. Fluid Mechanics and Thermodynamics of Turbomachinery. Oxford, UK: Butterworth-Heinemann; 2013.
[17] Wilson DG, Korakianitis T. The Design of High-Efficiency Turbomachinery and Gas Turbines. New Jersey: Prentice Hall; 2014.
[18] Ansys Design Modeler, Ansys Inc., <https://www.ansys.com/>.
[19] Ansys Turbogrid, Ansys Inc., <https://www.ansys.com/>.
[20] Ansys Fluent Solver, Ansys Inc., <https://www.ansys.com/>.
[21] REFPROP, NIST Reference Fluid Thermodynamic and Transport Properties Database, <https://www.nist.gov/srd/refprop>.
[22] F. R. Menter, “Two-equation eddy-viscosity turbulence models for engineering applications,” AIAA J., vol. 32, no. 8, pp. 1598–1605, 1994.
[23] Denton, J. D., Some Limitations of turbomachinery CFD, Proceedings of ASME Turbo Expo 2010: Power for Land, Sea, and Air, Glasgow, UK, 2010.